International Journal of Engineering & Technology, 7 (3.11) (2018) 48-51

International Journal of Engineering & Technology

Website: www.sciencepubco.com/index.php/IJET

Research paper

Structural Studies of Zno Nanostructures on Porous Silicon: Effect of Post-Annealing Temperature

Kevin Alvin Eswar[1,2,3*], Mohd Husairi Fadzillah Suhaimi[2,3], Muliyadi Gulilling[1,3], Zuraida Khusaimi[2,3], Mohamad Rusop[2] and Saifollah Abdullah[2,3]

[1]*Faculty of Applied Science, Universiti Teknologi MARA, Sabah Branch Tawau Campus, 91032 Tawau, Malaysia*
[2]*NANO-SciTech Centre, Institute of Science, Universiti Teknologi MARA, 40450 Shah Alam, Selangor, Malaysia*
[3]*Faculty of Applied Sciences, Universiti Teknologi MARA, 40450 Shah Alam, Selangor, Malaysia*
**Corresponding author E-mail:kevinalvin86@gmail.com*

Abstract

ZnO Nanostructures have been successfully deposited on of Porous silicon (PSi) via wet colloid chemical approach. PSi was prepared by electrochemical etching method. ZnO/PSi thin films were annealed in different temperature in the range of 300 °C to 700 °C. Surface morphology studies were conducted using field emission scanning microscopy (FESEM). Flower-like structures of ZnO were clearly seen at annealing temperature of 500 °C. The X-ray diffraction spectra (XRD) have been used to investigate the structural properties. There are three dominant peaks referred to plane (100), (002) and (101) indicates that ZnO has a polycrystalline hexagonal wurtzite structures. Plane (002) shows the highest intensities at annealing temperature of 500 °C. Based on plane (002) analysis, the sizes were in range of 30.78 nm to 55.18. In addition, it was found that the texture coefficient of plane (002) is stable compared to plane (100) and (101).

Keywords: *Structural properties; Flower-like ZnO; Porous silicon; Annealing temperature*

1. Introduction

Metal oxide thin films have been extensively studied in the last few decades. Zinc oxide (ZnO) is one of them. It becomes popular due to properties of a large exciton binding energy of 60 meV and and a wide band gap (E_g) of 3.37 eV [1]. In addition, good chemical and thermal stability, non-toxic material and high transparency in room temperature are additional advantages in devices fabrication [2]. There are various structures of ZnO have been produced such as nanoparticles, nanorods, nanowires, nano-flower and honey-comb [3-6]. The structure are highly depends on the methods applied such as hydrothermal, RF sputtering, sol-gel synthesis and pulsed laser ablation [7]. Among them, hydrothermal is the most practical for cost-effective method. In addition this method is controllable and implemented in low temperature. In substrate selection, silicon is the most popular due to its abundance in the earth crust. However, large mismatch between ZnO and silicon make it very challenging to deposits ZnO on silicon surface [8, 9]. As an alternative, modifications of silicon surface are required. The silicon surface modified into porous to make the surface contact become larger.

2. Method

Wet colloid chemical approach was employed to synthesis ZnO nanostructures on PSi. PSi was prepared using electrochemical etching. Then, the ZnO thin film was deposited on PSi using sol-gel spin coating method as a seeded. Flower-like ZnO nanostructures were grown on PSi via simple hydrothermal method. Zinc nitrate hexahydrate (Zn $(NO_3)_2.6H_2O$) was used as starting material while the hexamethylenetetramine (HMTA) as a stabilizer and dionized water as a solvent. The molarities of precursor were maintained at 0.2 M. PSi substrate was immersed into the ZnO precursor at 90 ℃ for 4 hours. It was followed by post-annealing heat treatment. The temperatures were varied from 300 °C to 700 °C. The field emission scanning microscopic (FESEM) was used to study the morphology of ZnO nanostructures. The structural property was investigated using X-ray diffraction (XRD) spectroscopy.

3. Results and Discussion

Surface morphologies were investigated using FESEM characterization. Fig.1 shows the FESEM images of PSi and ZnO nanostructures on seeded PSi. Samples were treated by different post-annealing temperature in range of 300 °C to 700 °C. ZnO nanostructures were agglomerate when annealed at 300 °C. The structures also cannot be identified. A flower-like structure has been produced at annealing temperature of 500 °C. It can be seen that the nano-flower is combination of ZnO nanorod. It was merges with adjacent nanostructures at post annealing temperatures of 700 °C to form of hexagonal island-like structures. The FESEM result shows that, post annealing temperatures are highly affecting the growth of ZnO nanostructures. Suggested that colloidal of ZnO have been formed within the solution. Furthermore, the growth of ZnO nanostructures in different structures may occur during post-annealing.

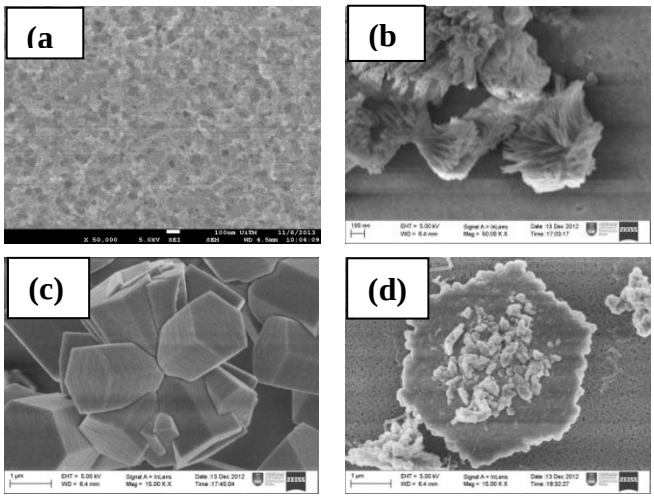

Fig. 1: FESEM images of (a) PSi and ZnO nanostructures deposited on seeded PSi with molarity of (b) 300 ℃ , (c) 500 °C and (d) 700 ℃

Fig.2 shows the XRD patterns of ZnO nanostructures treated with different annealing temperatures. Three dominant peaks referred to plane (100), (002) and (101) of ZnO nanostructures (JCPDS No: 36-1451) are appeared. Besides, plane of (102) and (100) are also seen in low intensity. This result indicates that ZnO has a polycrystalline hexagonal wurtzite structures [10]. Some impurities were found at annealing temperatures of 300 °C, 400 °C and 500°C which attributed by PSi substrate (JCPDS No: 17-0901) [11, 12]. This peak located in between plane of (100) and (002). The absence of PSi peak at annealing temperatures of 600 °C and 700 °C may be all surfaces may be covered by ZnO nanostructure at higher post-annealing temperature. Peak of plane (100) located at 32.08° to 32.21°, (002) located at 34.70° to 34.92° and (101) located at 36.52° to 36.72°. As can be seen, peak position slightly shifted to higher diffraction angle when annealing temperatures increased. The same phenomena have been found by Gao et. al. [13]. This is due to effect of strain within the crystalline.

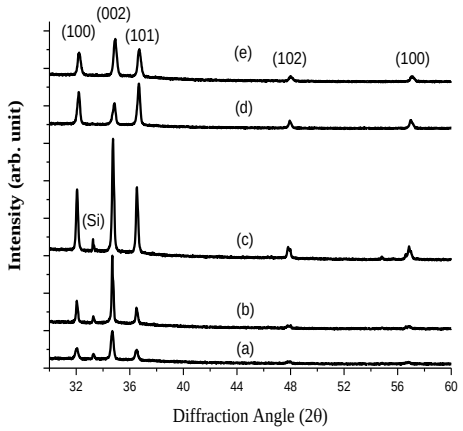

Fig. 2: XRD grating of ZnO nanostructures in different post-annealing temperatures of (a) 300 ℃, (b) 400 °C, (c) 500 °C, (d) 600 °C and (e) 700 ℃

Table 1 shows the plane distance, *d* and crystallite size, *D* in different annealing temperature. Plane distance of each plane in was calculated by Bragg's formula in Equation (1). Besides, an estimation of crystalline size, *D* based on plane distance for each plane is also calculated using Equation (2). The parameter of λ, *d*, and θ represents sources wavelength, plane distance and peak position in radian. In this study, 0.154 nm of Cu Kα radiation was used as sources [14].

$$\lambda = 2d\sin\theta \quad (1)$$

Scherrer's formula was used to estimate the crystalline size by using plane distance, *d* for each plane. It can be represented by

$$D = \frac{K\lambda}{\beta\cos\theta} \quad (2)$$

where *D, K,* λ*,* β*,* and θ represents crystallite size, Scherer's constant (0.9), X-ray wavelength, FWHM and peak position respectively [11]. This equation shows that crystallite size, *D* is directly influenced by the FWHM and peak position of each plane.

Table 1: FWHM of plane distance and crystallite size of plane (002) in different annealing temperatures

Annealing Temperatures (°C)	FWHM (°)	Plane distance, *D* (nm)	Size (nm)
300	0.223	0.2581	37.02
400	0.151	0.2581	55.18
500	0.170	0.2578	49.1
600	0.260	0.2569	32.11
700	0.270	0.2566	30.78

Generally, FWHM increases due to increase of due to increases of annealing temperatures. The increases of the FWHM are related to the decreases of crystallite size. The plane distance is highly dependent on peak position. The plane of (002) distance is consistent with Urgessa et al. by using high resolution transmission electron microscope [15].

Table 2 shows the lattice constant of '*a'* and '*c'*, Zn-O bond length, *L* and *u*, parameter used in bond length calculation in various molarity. As a reference, lattice constant of ZnO from JCPDS 36-1451 are $a_0 = b_0 = 0.32498$ nm and $c_0 = 0.52066$ nm. Lattice constant of '*a*' and '*c*' of the ZnO wurtzite structure can be calculated using the relation [14]

$$\frac{1}{d^2_{hkl}} = \frac{4}{3}\left(\frac{h^2+hk+k^2}{a^2}\right) + \frac{l^2}{c^2} \quad (3)$$

where d_{hkl} represents distance between adjacent planes in the Miller indices (*hkl*). Parameter of '*a'* and *'c'* are the lattice constant. The lattice constant '*a'* is obtained from plane (100) with relation

$$\frac{1}{d^2_{100}} = \frac{4}{3}\left(\frac{1}{a^2}\right) \quad (4)$$

while, the lattice constant '*c*' can be obtained from plane (002) with relation

$$\frac{1}{d^2_{002}} = \frac{4}{c^2} \quad (5)$$

From Equation (1), (4) and (5), the lattice constant '*a*' and '*c*' can be derived as

$$a = \frac{\lambda}{\sqrt{3}\sin\theta} \quad (6)$$

$$c = \frac{\lambda}{\sin\theta} \quad (7)$$

In order to find the bond length, *L* of Zn-O, lattice parameter 'a' and 'c' were used in the relation [16]

$$L = \sqrt{\left(\frac{a^2}{3} + \left(\frac{1}{2} - u\right)^2 c^2\right)} \quad (8)$$

Where,

$$u = \frac{a^2}{3c^2} + 0.25 \quad (9)$$

Lattice constant of 'a' and 'c', bond length, *L* and parameter *u* were summarized in Table 2. Lattice constant, bond length and *u* parameter were calculated by using Equation (2), Equation (8),

and Equation (9) respectively. Lattice constant was related to the plane distance of Miller indices plane. Besides, bond length is highly dependent on lattice constant and parameter *u*. Parameter *u* is related to the ratio of lattice constant 'a' and 'c'. The lattice constant 'a' and 'c' found may be reduced or higher compared to theoretical value found from referred JCPDS (36-1451) due to lattice strain of crystal. In case of lattice constant lower than theoretical, crystalline was compressed and expand if lattice constant is higher. Fig. 3 shows the texture coefficient, *TC* of peak (100), (002) and (101). In order to calculate the texture coefficient, *TC* following equation was used [17]

$$TC_{(hkl)} = \frac{\frac{I_{(hkl)}}{I_{0(hkl)}}}{\frac{1}{N}\sum_N\left(\frac{I_{(hkl)}}{I_{0(hkl)}}\right)} \quad (10)$$

where $I_{(hkl)}$ integrated intensities corresponding to plane (*hkl*) in this study, $I_{0(hkl)}$ is integrated intensities theoretically, and *N* is the number of diffraction peak. It can be seen that the texture coefficient of plane is increase consistently shows that the crystalline of ZnO grew with plane (002)-oriented.

Table 2: Lattice constant and bond length, *L* of based on peak (100), (002) and (101) in different annealing temperatures

Annealing Temperature (°C)	Lattice constant, (nm)	Bond Length, *L* (nm)	*u*
300	a= 0.3217	0.1959	0.3794
	c= 0.5163		
400	a = 0.3220	0.1960	0.3797
	c= 0.5163		
500	a = 0.3218	0.1959	0.3799
	c= 0.5155		
600	a = 0.3206	0.1952	0.3798
	c= 0.5138		
700	a = 0.3204	0.1949	0.3799
	c= 0.5131		

Hsu et al. have been studied the texture coefficient of ZnO nanostructure grown on PSi [12]. They have suggested that, preferred orientation is exists if the texture coefficient is more than 1. By referring the Equation (4.18), texture coefficients were calculated. In this case, three dominant peaks of (100), (002), and (101) were considered and analyzed. Figure 4.26 shows texture coefficient of ZnO nanostructures in different annealing temperature. As can be seen in Fig. 3, texture coefficients of (002) is more than 1 and stable except for annealing temperature of 600°C. This result shows preferred orientation of ZnO nanostructure growth is plane (002).

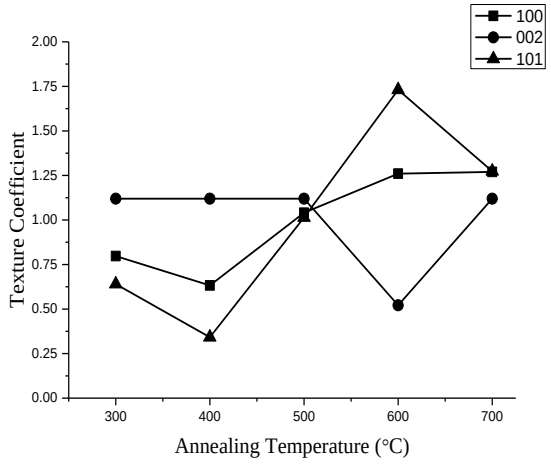

Fig. 3: Texture coefficient of ZnO nanostructures in different post-annealing temperatures of (a) 300 °C, (b) 400 °C, (c) 500 °C, (d) 600 °C and (e) 700 °C

4. Conclusion

ZnO nanostructures were successfully synthesized using hydrothermal method. Flower-like ZnO were deposited on PSi at annealing temperature of 500 °C. The crystalline size were found in range of 30.78 nm to 55.18 nm. Besides, the bond length, *L* is ~ 0.19 nm. In addition, based on texture coefficient, the preferred orientation of ZnO nanostructure growth is plane (002).

Acknowledgement

The authors would like to thank Universiti Teknologi MARA (UiTM) and also Malaysia Ministry of Higher Education for their support and funding from I-Rags Grant, file no: 600-RMI/IRAGS 5/3 (20/2015).

References

[1] K. Eswar, J. Rouhi, H. Husairi, M. Rusop, and S. Abdullah, "Annealing heat treatment of ZnO nanoparticles grown on porous Si substrate using spin-coating method," *Advances in Materials Science and Engineering*, vol. 2014, 2014.

[2] J. Ghosh, R. Ghosh, and P. K. Giri, "Tuning the visible photoluminescence in Al doped ZnO thin film and its application in label-free glucose detection," *Sensors and Actuators B: Chemical*, vol. 254, pp. 681-689, 2018/01/01/ 2018.

[3] V. S. Bhati, S. Ranwa, M. Fanetti, M. Valant, and M. Kumar, "Efficient hydrogen sensor based on Ni-doped ZnO nanostructures by RF sputtering," *Sensors and Actuators B: Chemical*, 2017/08/18/ 2017.

[4] K. A. Eswar, A. Azlinda, H. F. Husairi, M. Rusop, and S. Abdullah, "Post annealing effect on thin film composed ZnO nano-particles on porous silicon," *Nano Bulletin*, vol. 2, p. 130212, 2013.

[5] Y. Feng, G. Wang, J. Liao, W. Li, C. Chen, M. Li, *et al.*, "Honeycomb-like ZnO Mesoporous Nanowall Arrays Modified with Ag Nanoparticles for Highly Efficient Photocatalytic Activity," *Scientific Reports*, vol. 7, p. 11622, 2017/09/14 2017.

[6] A. Shkurmanov, C. Sturm, H. Franke, J. Lenzner, and M. Grundmann, "Low-Temperature PLD-Growth of Ultrathin ZnO Nanowires by Using Zn x Al1−x O and Zn x Ga1−x O Seed Layers," *Nanoscale Research Letters*, vol. 12, p. 134, 2017.

[7] K. Eswar, J. Rouhi, F. Husairi, R. Dalvand, S. A. Alrokayan, H. A. Khan, *et al.*, "Hydrothermal growth of flower-like ZnO nanostructures on porous silicon substrate," *Journal of Molecular Structure*, vol. 1074, pp. 140-143, 2014.

[8] K. A. Eswar, A. Lepit, R. Rasmidi, F. Husairi, A. Afaah, N. Aadilla, *et al.*, "Seeded Porous Silicon Preparation as a Substrate in the Growth of ZnO Nanostructures," in *Applied Mechanics and Materials*, 2015, pp. 626-631.

[9] R. S. Dariani and M. Zabihipour, "Effect of electrical behavior of ZnO microparticles grown on porous silicon substrate," *Applied Physics A*, vol. 122, p. 1047, 2016// 2016.

[10] X. T. Zhang, Y. C. Liu, Z. Z. Zhi, J. Y. Zhang, Y. M. Lu, D. Z. Shen, *et al.*, "Temperature dependence of excitonic luminescence from nanocrystalline ZnO films," *Journal of Luminescence*, vol. 99, pp. 149-154, 2002.

[11] S. K. Min, G. Y. Kwang, L. Jae-Young, K. Soaram, N. Giwoong, Y. K. Do, *et al.*, "Nanocrystalline ZnO Thin Films Grown on Porous Silicon by Sol-gel Method and Effects of Post-annealing," *Journal of the Korean Physical Society*, vol. 59, p. 346, 2011.

[12] H. C. Hsu, C. S. Cheng, C. C. Chang, S. Yang, C. S. Chang, and W. F. Hsieh, "Orientation-enhanced growth and optical properties of ZnO nanowires grown on porous silicon substrates," *Nanotechnology*, vol. 16, pp. 297-301, Feb 2005.

[13] K. Gao, Q. Li, Z. Hu, W. Yu, J. Sun, N. Xu, *et al.*, "Correlation between structure and photoluminescence of c-axis oriented nanocrystalline ZnO films and evolution of photo-generated excitons," *Solar Energy Materials and Solar Cells*, vol. 96, pp. 117-123, 2012.

[14] A. Khorsand Zak, W. H. Abd. Majid, M. E. Abrishami, and R. Yousefi, "X-ray analysis of ZnO nanoparticles by Williamson–Hall and size–strain plot methods," *Solid State Sciences*, vol. 13, pp. 251-256, 2011.

[15] Z. N. Urgessa, O. S. Oluwafemi, E. J. Olivier, J. H. Neethling, and J. R. Botha, "Synthesis of well-aligned ZnO nanorods on silicon

substrate at lower temperature," *Journal of Alloys and Compounds*, vol. 580, pp. 120-124, 2013.
[16] M. S. Kim, S. Kim, G. Nam, D.-Y. Lee, and J.-Y. Leem, "Effects of growth temperature for buffer layers on properties of ZnO thin films grown on porous silicon by plasma-assisted molecular beam epitaxy," *Optical Materials*, vol. 34, pp. 1543-1548, 2012.
[17] M. S. Kim, K. G. Yim, S. Kim, G. Nam, and J.-Y. Leem, "White light emission from nano-fibrous ZnO thin films/porous silicon nanocomposite," *Journal of Sol-Gel Science and Technology*, vol. 59, pp. 364-370, 2011.